Journal Pre-proofs

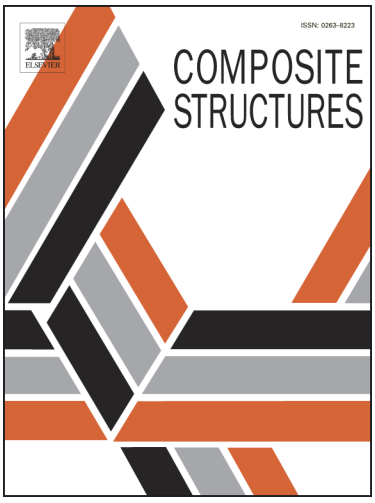

Damage and energy absorption behaviour of composite laminates under impact loading using different impactor geometries

Yuzhe Ding, Jun Liu, Zoe E.C. Hall, Richard A. Brooks, Haibao Liu, Anthony J. Kinloch, John P. Dear

PII: S0263-8223(23)00605-0
DOI: https://doi.org/10.1016/j.compstruct.2023.117259
Reference: COST 117259

To appear in: *Composite Structures*

Received Date: 25 January 2023
Revised Date: 2 May 2023
Accepted Date: 13 June 2023

Please cite this article as: Ding, Y., Liu, J., Hall, Z.E.C., Brooks, R.A., Liu, H., Kinloch, A.J., Dear, J.P., Damage and energy absorption behaviour of composite laminates under impact loading using different impactor geometries, *Composite Structures* (2023), doi: https://doi.org/10.1016/j.compstruct.2023.117259

Damage and energy absorption behaviour of composite laminates under impact loading using different impactor geometries

Yuzhe Ding [a], Jun Liu [a], Zoe E.C. Hall [a], Richard A. Brooks [a], Haibao Liu [b,*],

Anthony J. Kinloch [a], John P. Dear [a,*]

[a] *Department of Mechanical Engineering, Imperial College London, SW7 2AZ, UK*

[b] *Centre for Aeronautics, Cranfield University, MK43 0AL, UK*

Correspondence to: Dr Haibao Liu (haibao.liu@cranfield.ac.uk) and Prof John Dear (j.dear@imperial.ac.uk)

Abstract

The present paper compares the damage and energy absorption behaviour of composites subjected to low-velocity impact using different frontal geometries for the impactor, with the composites possessing a layup of $[0_2/90_2]_{2s}$. In this study, the rigid impactors with either round-nosed or flat-ended frontal geometry are employed to perform drop-weight tests at various impact energies ranging from 10 to 30 J. The measured loading response and energy absorption are analysed and compared. Additionally, the types and extent of impact-induced damage in the composite specimens are assessed via ultrasonic C-scan, optical microscopy (OM) and scanning electron microscopy (SEM) studies. It is shown that the impact energy threshold for damage initiation is greater than 20 J when using the flat-ended impactor but is less than 10 J when using the round-nosed impactor. In both cases, delamination initiates between the plies in the composite laminate. However, for the flat-ended impactor, the damage behaviour of the fibres exhibits kinking fracture, which differs from the pull-out fibre-fracture caused by the round-nosed impactor. These differences in behaviour are attributed to impactor/composite contact geometry effects which leads to different extents of indentation damage, which in turn directly affects the degree of delamination and fibre damage in the composite.

Keywords: Composite laminates; Low-velocity impact; Impactor geometry; Ultrasonic C-scan; Scanning electron microscopy (SEM)

1. Introduction

Carbon-fibre reinforced-polymer (CFRP) composites possess excellent in-plane strength and stiffness properties and have been extensively employed in the latest generation of passenger aircraft for fuselage, wings, engine cowls, ailerons and spoilers [1-3]. However, during manufacture and service, these structures are vulnerable to damage caused by impact events, such as dropped tools and runway debris [4, 5].

The profile of the front face of the impactor has been shown to be of importance in determining the position and shape of the initial damage, and the way in which the damage then develops in a composite material [6-26]. For example, Cantwell, Morton and other researchers have shown how the dynamic response and damage development of CFRP structures can be considerably influenced by the frontal geometry of the impactor [6-10]. Indeed, Zhou et al. [11] have found that for a round-nosed impactor the initial failure of the composite was associated with indentation at the impact point and the initiation of matrix cracking. These events are then followed by interlaminar damage, i.e. delaminations, developing between the plies. In contrast, for a flat-ended impactor, the plies were sheared around the edge of the impactor face that contacted the composite and then delaminations developed. In both cases, depending on the impactor profile and the impact energy, fibre fracture can also occur. Mines et al. [12] found that invariably the damage induced when using a relatively sharp impactor was more localised. In contrast, a blunter impactor produced a larger delamination area. These findings have been substantiated more recently by work reported by Icten et al. [13] and Sevkat et al. [14], who performed a series of impact tests using woven- and hybrid-fibre composites and found similar effects.

Mitrevski et al. [15] have reported the effects of the frontal shape of the impactor on the impact behaviour of woven CFRP composites. Their studies involved the low-velocity impact of the composites using round-nosed (hemispherical), ogival and conical head-shaped impactors at impact energies of 4 J and 6 J. They found that the energy absorbed by the specimen was the highest for the relatively sharp conical impactor, which also resulted in the largest indentation depth in the composite surface. However, the peak load was greatest for the hemispherical impactor, which also produced the shortest contact duration. In a subsequent paper, Mitrevski et al. [16] reported that different impactor head-shapes produced different extents of the various types of damage that were observed, such as fibre breakage, matrix cracking and delamination, which affected the residual properties of the composite. It was found that the relatively blunt round-nosed impactor produced the largest damage area and the type of damage was dominated by delamination. These conclusions were supported by the work of Kurşun et al. [17] who found that a sharper impactor was more likely to generate permanent indentation deformation in the surface of the composite material at the impact point, with their research considering impact energies of 29 and 44 J. In contrast, a flat-ended impactor was more likely to generate regions of localised brittle damage. Similar findings were also reported by Elaldi et al. [18] who found that a flat-ended impactor generated the largest delamination area at higher levels of impact energy. Kazemianfar et al. [19] studied the effects of conical, round-nosed and flat-ended impactors on 3D woven composites and they concluded that the sharper impactors resulted in a lower damage threshold load. Nevertheless, the damage initiation time for the impact event was not dependent on the impactor shape and as the impactor tip became blunter the maximum indentation into, and the degree of damage of, the composite decreased. Further, Dhakal et al. [20] also demonstrated that composites struck using a round-nosed impactor were able to endure

higher impact loads than when hit using sharp, conical impactors. The round-nosed impactor induced more extensive damage in the composite, which corresponded to the composites ability to endure higher loads, and absorb more energy, when struck by a relatively blunt, round-nosed impactor, compared to specimens tested using the relatively sharp conical impactors. Work by Mahesh et al. [21] and Liu et al. [22] has also shown that using a flat-ended shaped impactor resulted in more extensive damage in the composite compared to other frontal geometries of impactors.

It is worth noting that identification of the damage mechanisms of impacted composite panels can provide very useful information as to the type and sequence of damage initiation and propagation. Several research groups [11, 23-25] have observed the presence of fractured fibres and other damage mechanisms using scanning electron microscopy (SEM) and concluded that slight changes in the impact test parameters may cause noticeable differences in the type and extent of the damage mechanisms at the micro-scale. Finally, from the above, it appears that a relatively sharp impactor can readily cause visible damage, for example by leaving a clear indentation mark on the surface of the composite or even by complete penetration through the composite specimen. On the other hand, the damage caused by using round-nosed and flat-ended impactors typically gives rise to 'barely visible impact damage' (BVID) on the surface of the impacted composite. The term BVID means that no clear indentation, or other damage, of the composite can be readily observed, even though the damaged area in the composite may be more extensive from using a relatively blunt frontal geometry for the impactor. Clearly, when only a visual inspection of a composite structure takes place, the presence of BVID presents a relatively difficult challenge for the engineer to detect and then repair, as necessary.

To assist in resolving some of the remaining questions and discrepancies arising from the above previous work, our research [26] in the past has undertaken a limited study on the effects of the front face geometry of the impactor at relatively low impact velocities on cross-ply CFRP panels using rigid round-nosed and flat-ended impactors. The impactor geometry was indeed found to affect the extent and shape of the delaminations that resulted in these composite laminates. However, only two impact energies, i.e. 15 and 45 J, were employed in this past work. Thus, to obtain more detailed results, so as to enable the impact response and the type and extent of damaged to be mapped, in the present study CFRP panel specimens are tested at a far wider range of impact energies, i.e. 10, 15, 20, 25 and 30 J. The damage maps, load-time and load-displacement traces and trends in the absorbed impact energy are measured when using either the round-nosed or the flat-ended rigid impactor. In addition, the present study has now used ultrasonic C-scanning, optical microscopy. scanning electron microscopy and white light interferometry to identify the extent of indentation and the detailed damage mechanisms induced by using the two different impactor geometries over a wide range of impact energies.

2. Materials and Experimental Details

Unidirectional carbon-fibre/epoxy-matrix prepreg (MTC510-UD300-HS-33%RW), supplied by SHD Composites Ltd, UK, was used to fabricate the test specimens. This prepreg contains T700 carbon fibres at a volume fraction of 60% and panels were laid-up in a cross-ply configuration of $[0_2/90_2]_{2s}$. Large panels were manufactured via an autoclave consolidation process. They were cured at a constant temperature and pressure of 110℃ and 6 bars,

respectively, for a dwell-time of 120 minutes, followed by cooling down to room temperature at 2°C per minute. These large panels had a nominal thickness of 4.6 mm and were cut into standard test panels with dimensions of 150 mm x 100 mm, as schematically shown in Fig. 1, which follows the ASTM Standard 7136 [27]. All specimens were inspected prior to testing by using an ultrasonic C-scanner, supplied by Sonatest Ltd, UK, and they were then assessed again after impact.

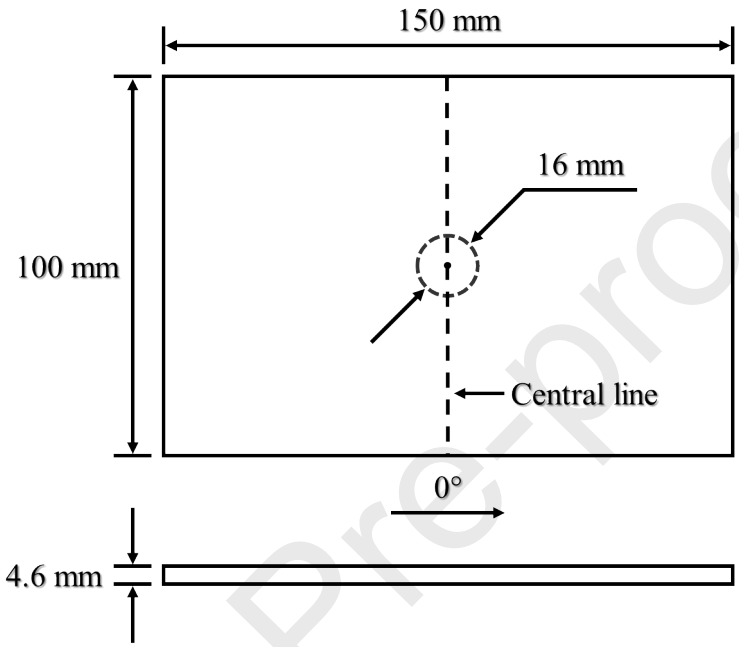

Fig. 1. Dimensions of the test composite panels. The dashed circle of diameter 16 mm indicates the circumference of the hemispherical front of the round-nosed impactor and the contact area for the flat-ended impactor, which is circular in shape, see Fig. 2.

Fig. 2 shows the two types of rigid impactor tup, for the round-nosed impactor with a hemispherical end and the flat-ended impactor with a frontal circular area, used in the present study. Both impactors were manufactured from stainless-steel with a diameter of 16 mm and their masses were 5.265 and 5.255 kg, respectively.

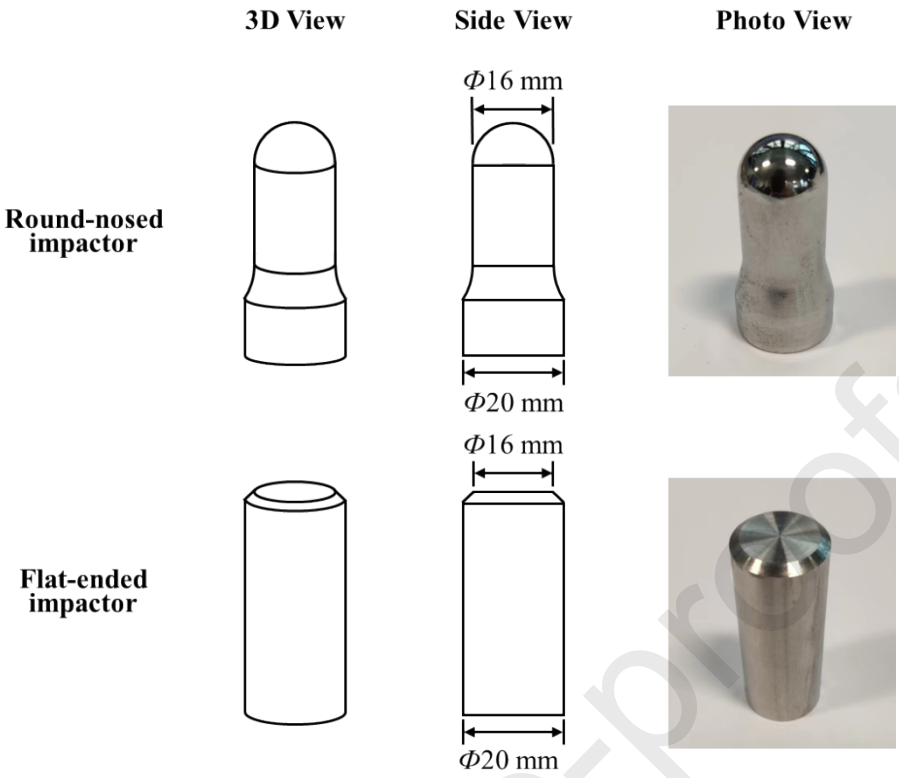

Fig. 2. Sketches and photographs of the round-nosed and the flat-ended rigid impactor tups.

The main research interest in the present work was low velocity impacts by a large mass, where the material can respond quasi-statically to the impact threat. It is difficult to give a precise definition for this statement, as it depends on the specimen material and its shape, but generally impact velocities of a few $m{\cdot}s^{-1}$ are considered to represent low velocity impact conditions. In this study, low velocity impact tests, with a maximum impact velocity of 10 $m{\cdot}s^{-1}$, were implemented by employing an 'Instron 9340' drop-tower, supplied by CEAST, Italy (see Fig. 3). It is equipped with a data acquisition system, which connects to a photoelectric sensor, and a load cell with a capacity of 22 kN and a data sampling rate of 500 kHz. These elements allow the impact velocity, impact load and displacement of the specimen to be obtained. Test panels were clamped in the lower part of the tower, using four toggle clamps, onto a steel fixture with a cut-out window of 125 mm x 75 mm. An appropriate height was set to deliver the range of impact energies from 10 to 30 J for the impactors, which was calculated as determined by the impact energy required. When the released impactor passed through the sensor's light beam, the data acquisition system was triggered to record the time it took from the sensor to the impact point. The impact velocity was then calculated based on the measured time and the distance between the sensor and the impact point. The residual velocity was obtained in the same way. The load versus time trace was outputted when the impactor touched the specimen. Finally, the displacement was calculated, via the software supplied by CEAST, by double integration of the load versus time response using Newton's Second Law. The test equipment employed a catching system which was activated after the first impact to avoid multiple impacts to the composite panel specimens. To study the reproducibility of the test procedures, impact tests at each energy level were repeated at least in duplicate.

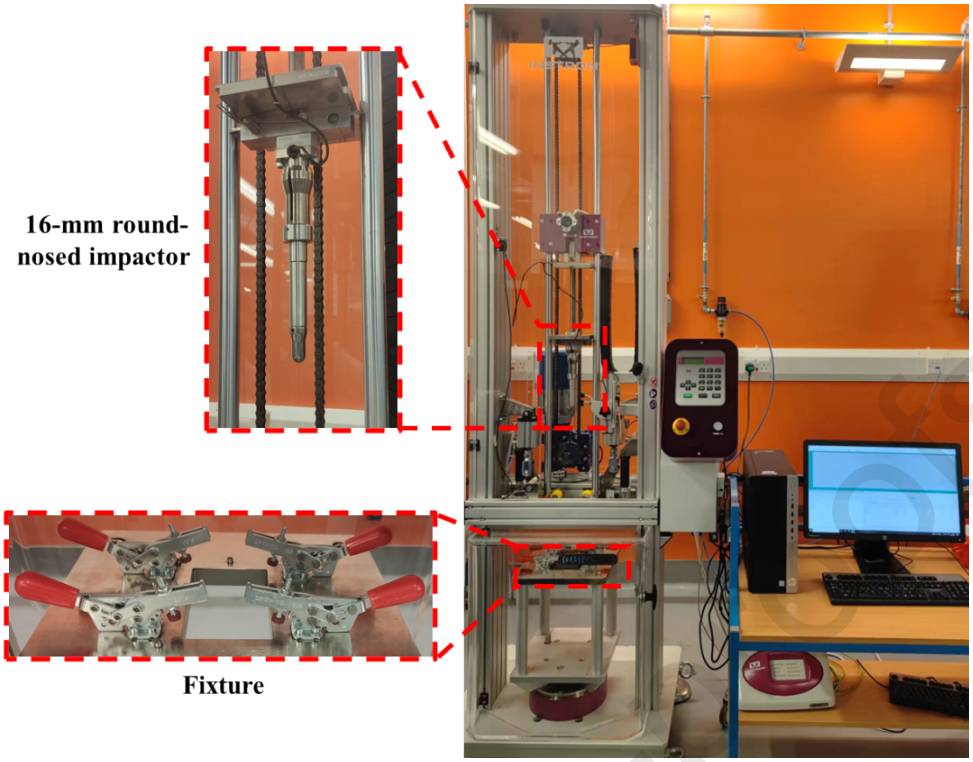

Fig. 3. The experimental set-up for the drop-weight impact experiments.

The post-impacted specimens were first C-scanned to record the delamination area by using a portable ultrasonic scanner 'Prisma', supplied by Sonatest Ltd., UK. They were subsequently sectioned along the central line of the panel (see Fig. 1) using a 'Brillant 220' cutting machine, provided by QATM, Germany. To prevent additional damage being introduced during cutting, a 0.5 mm thick diamond cut-off wheel, which has a precision of 1 μm, was used. The machine was set to have a forward speed of 0.2 mm per second with a rotational speed of 4000 rpm. The damage in the sectioned panels was characterised using a field emission gun SEM 'MIRA', supplied by TWSCAN, Czech.

3. Results and Discussion

3.1. Dynamic response

The loading responses for the composite panels subjected to an impact using either the round-nosed or the flat-ended impactors are shown in Figs. 4 and 5. It can be seen that, for all the impact energies, the flat-ended impactor resulted in a higher peak load, shorter contact duration and lower displacement when compared with the round-nosed impactor.

The small amplitude sinusoidal oscillations on the initially-rising part of the load versus time and load versus displacement curves, as evident in Fig. 4 and 5, are indicative of mass-spring oscillations [29-32]. They occur when using both the flat-ended and round-nosed impactors at all impact energies. However, in some cases, there are also more significant load drops, which are indicative of the initiation of damage in the composite specimens. After the first point of a significant load drop, there is a change in gradient and also oscillations in the load, which are associated with the propagation of various damage mechanisms in the composite material, e.g. matrix cracking, delamination and fibre fracture, as observed by Bienias et al. [33]. For instance, from Figs. 4 and 5, it should be noted that, for the round-nosed impactor, there is a distinct load drop at approximately 5 kN for all impact energies. This suggests that damage initiates at the same load value at all impact energies, i.e. from 10 to 30 J. In contrast, for the flat-ended impactor the load drop is more significant and occurs at a higher load of approximately 12 kN, but only for the two tests using the highest impact energies, i.e. 25 and 30 J. Clearly, the load required for damage to initiate is dependent on the contact geometry, as well as the composite material properties.

As noted above, for the flat-ended impactor, load drops were only apparent for impact energies of 25 and 30 J. Once a significant load drop is observed, at approximately 12 kN, the load traces do not climb to a higher load level, see Figs. 4 and 5. This implies that the damage initiation load for these impact tests is near the peak load. This, in turn, means the panel is not able to carry a higher load once the initial damage has occurred. Beyond the load initiation point, the traces for the flat-ended impactor tests exhibited extreme oscillations for these relatively high impact energies of 25 and 30 J. During these impact events, the overall stiffness significantly decreased due to the propagation of extensive impact-induced damage, such as matrix cracking, delaminations and fibre fracture, as discussed later. Moreover, for the flat-ended impactor tests at 25 and 30 J, the load traces have many noticeable vibrations during the unloading phases for both the load versus time and load versus displacement traces. For the lower impact energies of 10, 15 and 20 J, in the flat-ended impactor tests, the maximum load does not reach the damage initiation load of approximately 12 kN and, for this reason, there is no significant load drop.

A major reason for the differences in the load traces for the round-nosed impactor and the flat-ended impactor tests is that the round-nosed impactor is far more likely to cause an indentation in the impacted face of the CFRP, compared to the flat-ended impactor. This, in turn, significantly affects the initiation and propagation of impact-induced damage in the CFRP. These important aspects are discussed in more detail below.

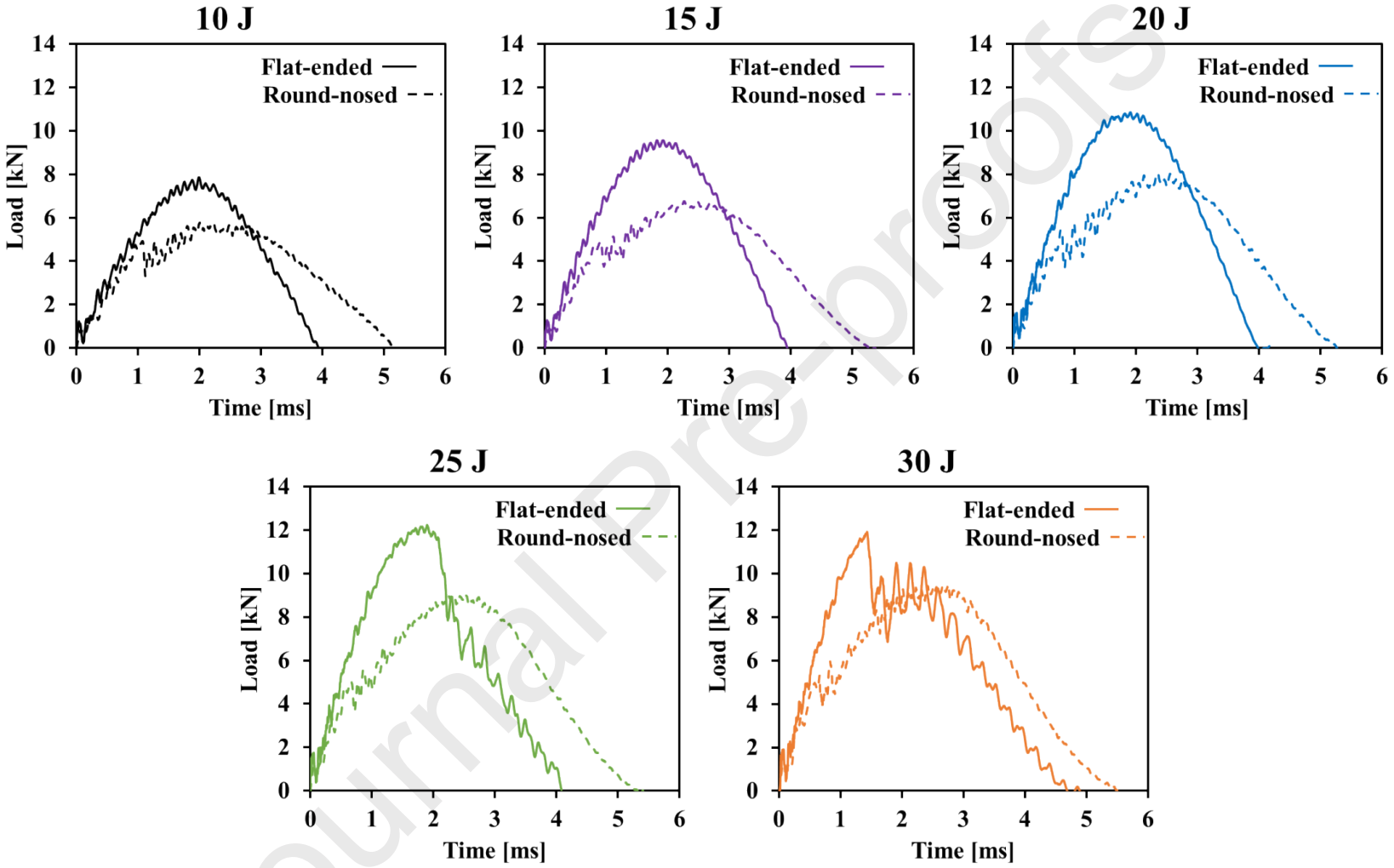

Fig. 4. Comparison of load versus time traces for the impact tests obtained from using either the round-nosed or the flat-ended impactor at impact energies of 10, 15, 20, 25 and 30 J, respectively.

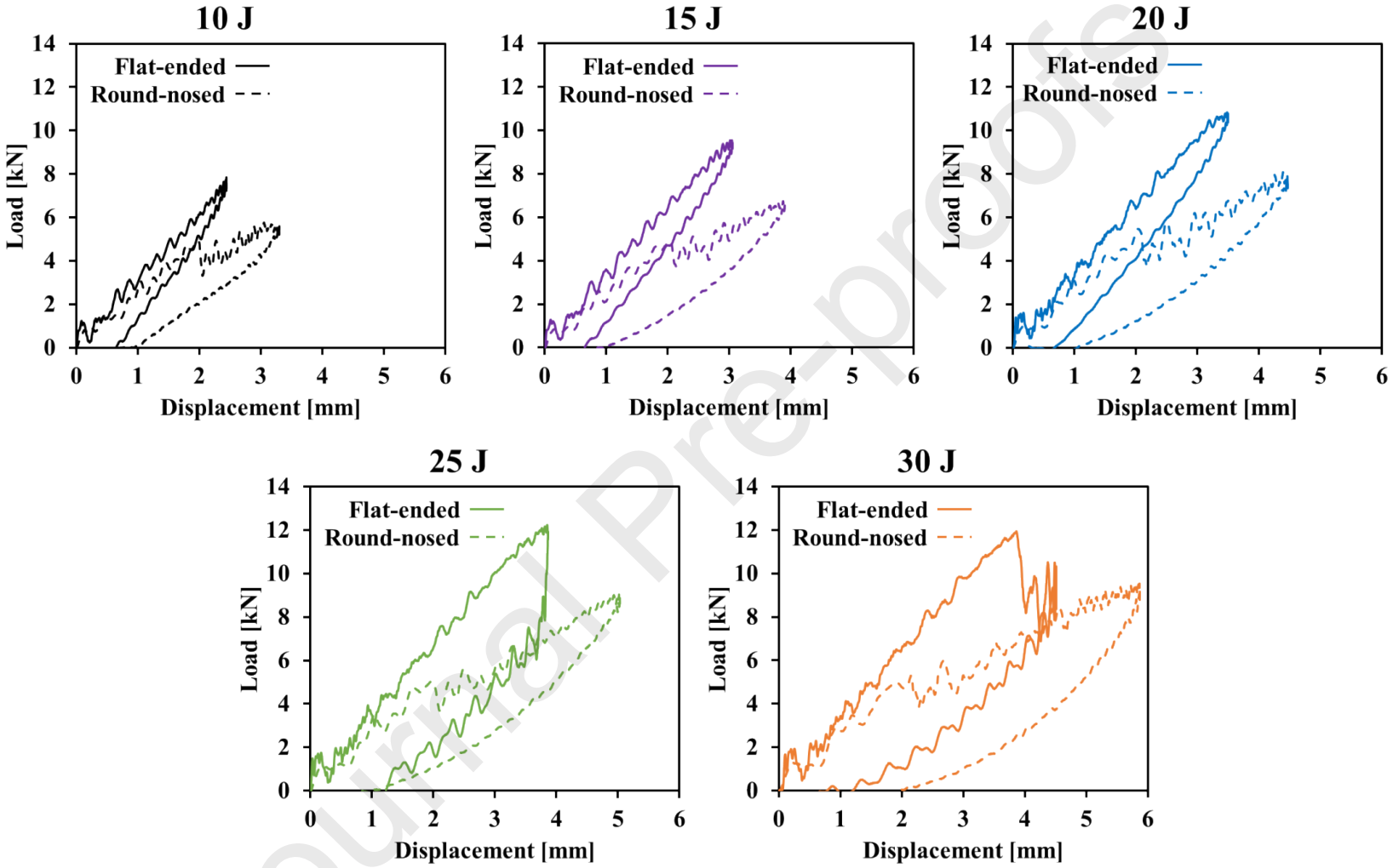

Fig. 5. Comparison of load versus displacement traces obtained for the impact tests obtained from using either the round-nosed or the flat-ended impactor at impact energies of 10, 15, 20, 25 and 30 J, respectively.

3.2. Delamination damage

Fig. 6 shows the C-scan images with the delamination at each ply interface colour-coded so that a blue delamination is near the rear surface and a red delamination is near the front, i.e. impacted surface. The dark blue colour corresponds to an ultrasonic reflection from the lowermost surface of the specimen, rather than a delamination. Each delamination has a characteristic peanut shape orientated along the fibre direction of the ply beneath the interface. The footprint delamination areas, given in the bottom left of each C-scan image in Fig. 6, are determined by counting the number of pixels which are not dark blue to give an area in mm^2. In the case of the round-nosed impactor tests, the delamination footprint corresponds to the whole area contained within the dashed white line. However, for the flat-ended impactor tests, there is a central zone of where no delamination occurs directly under the impact point of the flat-ended impactor, and this is not counted in the footprint delamination area. (Previous research by Liu et al. [26, 28] has shown that that the value of the footprint delamination area so deduced would be expected to vary by ± 5% from undertaking replicate tests.)

Delamination damage in the composite panel specimens impacted by the round-nosed impactor can be detected at all the impact energies, i.e. 10 to 30 J, and the footprint delamination area displays a near-linear growth with impact energy, see Fig. 7. In contrast, no delamination was detected in the panels impacted by the flat-ended impactor at the energy levels of 10, 15 and 20 J, whilst considerable delamination was detected for the 25 and 30 J impact energy levels, see Figs. 6 and 7. This observation agrees with the appreciable load drops seen on the load-time and load-displacement traces for only the 25 and 30 J impact energy levels. Fig. 7 also shows the delamination growth rate per unit increase in impact energy, i.e. the footprint delamination area divided by the increase in the impact energy. This parameter is highest for the flat-ended impactor at an impact energy of 25 J, giving a delamination growth rate of about 400 mm^2/J. For the round-nosed impactor, the delamination growth rate, at an impact energy level of 15 J, is about 100 mm^2/J and decreases progressively with increasing impact energy.

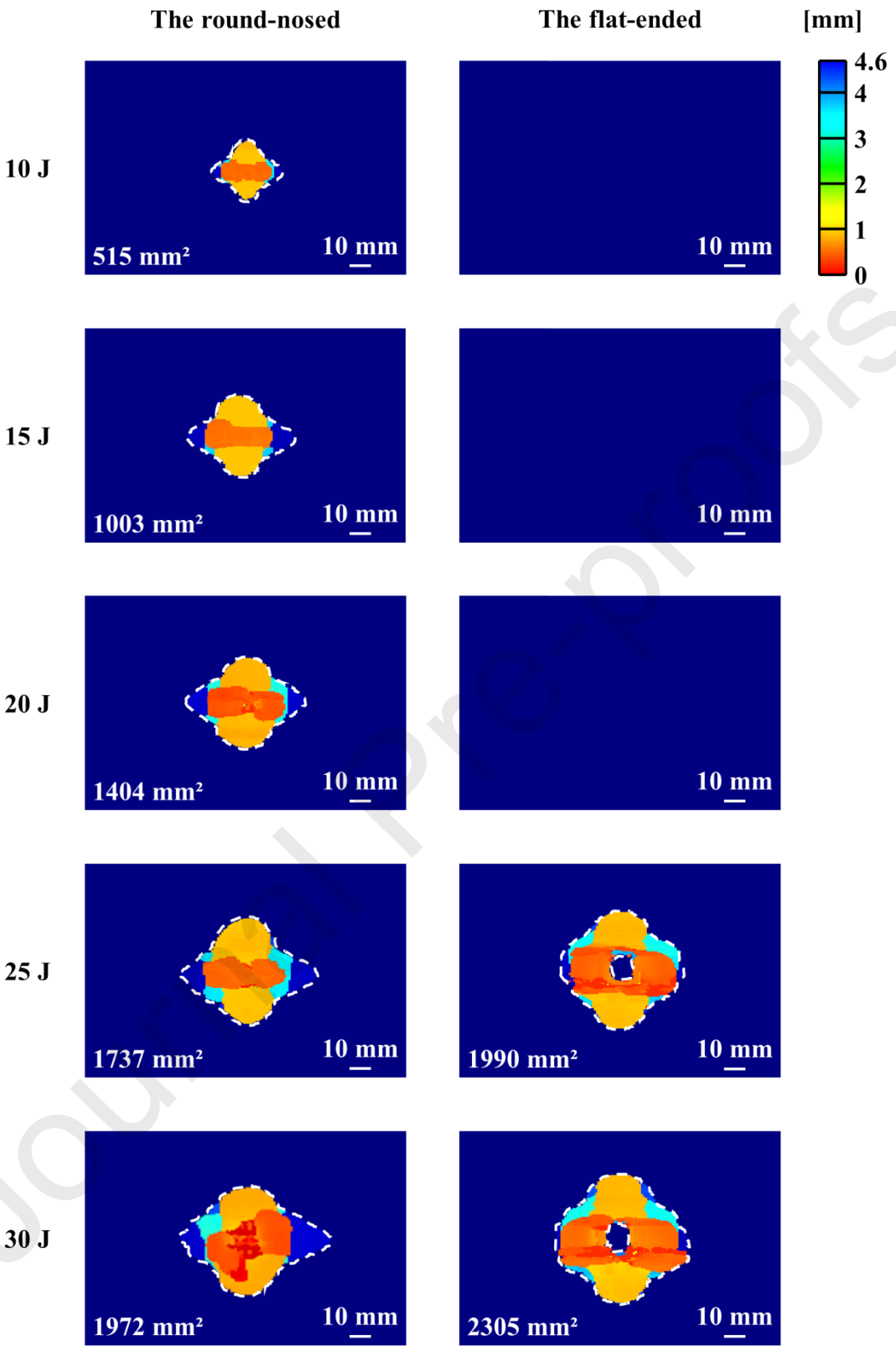

Fig. 6. C-scan maps obtained from the round-nosed and flat-ended impact tests performed at impact energies of 10, 15, 20, 25 and 30 J, respectively. (The footprint delamination is highlighted by white dashed lines and its area is given in the bottom left).

Figs. 6 and 7 clearly show that the flat-ended impactor causes severe delamination at the higher impact energies, i.e. 25 and 30 J. The size of the delaminations is almost equal at each ply interface through the thickness of the CFRP specimen in the flat-ended impactor tests where damage is detected. Also, there is no evidence of delamination immediately beneath the impactor at the central impact point, as indicated by the dark blue region in Fig. 6, which is an ultrasonic reflection from the rear surface. In contrast, for the round-nosed impactor cases, the size of the delaminations at each ply interface through the thickness increase in area from the front to the rear face of the specimen for all the impact energies studied.

For the round-nosed impact, due to the point contact between the impactor and target, a stress concentration arises under the impactor tip. This leads to the composite panel specimen being prone to indentation, as discussed in detail below, leading to matrix damage and delamination occurring at an impact energy as low as 10 J. Since the degree of indentation increased with impact energy, the extent of delaminations exhibited a relatively stable growth compared to when the flat-ended impactor is used, see Fig. 7.

For the flat-ended impact, the composite panels were subjected to shear stresses from the impactor periphery, which are distributed due to the surface contact between the impactor and the CFRP panel specimen. Moreover, carbon fibre has excellent shear strength and so the composite panels deformed mainly elastically upon impact at the lower impact energies, resulting in the absence of delaminations under the flat-ended impacts at energies of less than, or equal to, 20 J. However, for an impact energy of 25 J and above, associated shear deformation was induced once the threshold of shear strength was reached. This led to the dramatic growth of delaminations at lower ply interfaces where both shear and tensile stresses are present. At an impact energy of 25 and 30 J, since the flat-ended impact was dominated by shear stress and the induced tensile stresses, intralaminar microcracking damage caused by the associated tensile stresses initiated within the composite panel. Therefore, for the flat-ended impacts, at impact energies at 25 and 30 J, the composite panels mainly absorbed the impact energy via delamination and exhibited a larger area of delamination than the round-nosed impacts.

In Fig. 7, these differences in behaviour for the round-nosed and flat-ended impactor tests are identified by plotting the delamination area and its associated growth rate on a single plot. There is a slight reduction in the growth rate when using the round-nosed impactor, indicating that there is potential for the growth rate for round-nosed impactor to achieve a plateau. However, for the reasons stated above, the flat-ended impactor tests shows a dramatic increase and then a fall in the growth rate for impact energies of 25 and 30 J.

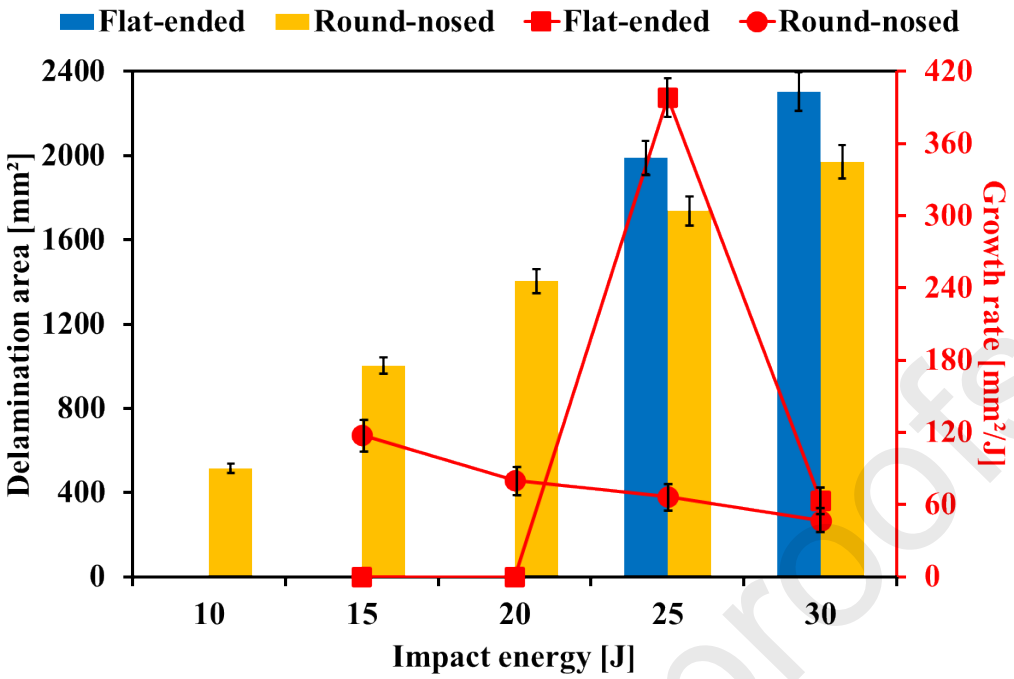

Fig. 7. The variation of the footprint delamination area with impact energy for both frontal shapes of impactors. The corresponding delamination area growth rate is shown on the right-hand y-axis, with red squares for the flat-ended and red circles for the round-nosed impactor.

3.3. Energy absorption

The overall results from assessing the impact behaviour are summarised in Table 1 for both the flat-ended and round-nosed impactors. This is with the impact energy absorbed by the CFRP panel, E_a, being given by:

$$E_a = \frac{1}{2}m(v_i^2 - v_r^2) \quad (1)$$

where m is the mass of the impactor, and v_i and v_r are the initial impact velocity and residual velocity, respectively. Fig. 8 shows a comparison between the energy absorption from using the flat-ended or the round-nosed impactor. For the round-nosed impactor, the absorbed energy is approximately linear with increasing impact energy, which agrees with the linear increase of delamination area observed in Fig. 7. It is notable that the absorbed energy from using the flat-ended impactor is lower than for the round-nosed impactor when the impact energy is less than about 20 J. However, for the flat-nosed impactor above an impact energy of 20 J, there is a dramatic increase in the absorbed energy which corresponds to the increase in delamination area observed in Fig. 7. In addition to energy absorption by delaminations occurring, there are other energy absorption mechanisms associated with elastic stored strain-energy, which is then dissipated as damped vibrational energy, and plasticity as well as other matrix and fibre-failure mechanisms which the C-scan technique does not visualize. There are also frictional losses at the support points of the composite panel and these will contribute to energy absorption. When the impact energy reaches 25 J, the flat-ended impactor tests exhibit a larger delamination area than the round-nosed impactor tests, i.e. about 15% higher at 25 J and 19% higher at 30 J. This

results in the absorbed energy in the flat-ended impactor tests surpassing that recorded for the round-nosed impactor tests for impact energy values greater than 25 J.

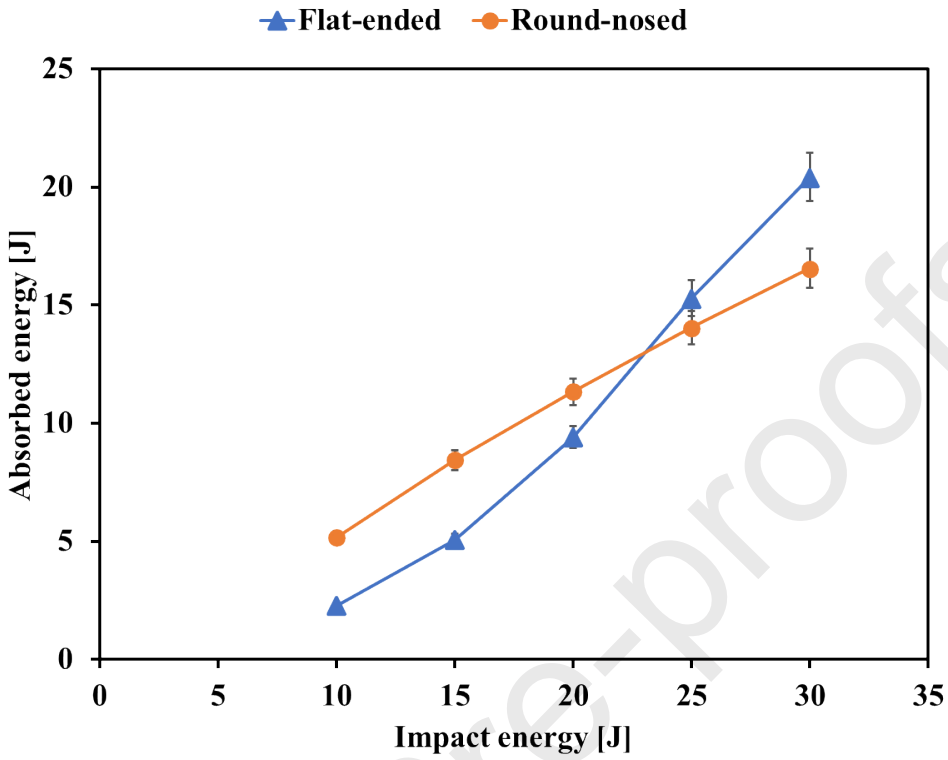

Fig. 8. Absorbed energies versus the impact energy from using the flat-ended and the round-nosed impactors.

Table 1. Summary of results obtained from CFRP panel specimens subjected to impact by the round-nosed or the flat-ended impactor. (Reproducibility for the delamination footprint area is typically ± 5%).

	Impact energy (J)	Peak load (kN)	Maximum out-of-plane displacement (mm)	Length of delamination for uppermost delamination (mm)	Ratio of delamination length for uppermost and lowermost delamination	Footprint delamination area (mm^2)	Absorbed energy (J)
Round-nosed impactor	10	5.7	3.3	24	0.71	515	5.2
	15	6.8	3.9	31	0.63	1003	8.4
	20	8.1	4.5	36	0.66	1404	11.3
	25	9.0	5.0	39	0.61	1737	14.0
	30	9.5	5.9	40	0.55	1972	16.6
Flat-ended impactor	10	7.8	2.5	–	–	–	2.3
	15	9.6	3.1	–	–	–	5.1
	20	10.8	3.5	–	–	–	9.4

	25	12.2	3.9	50	0.90	1990	15.3
	30	11.9	4.5	55	0.90	2305	20.4

3.4. Damage mechanisms

As observed in Fig. 6, and summarised in Table 1, for the round-nosed impactor, the maximum length of delamination for the uppermost delamination, i.e. nearest to the impacted face, increases steadily from 24 to 40 mm as the impact energy is increased. Additionally, the ratio of the uppermost to the lowermost delamination length decreases from 0.71 to 0.55. However, for the flat-ended impactor for the same impact energies of 25 and 30 J, the uppermost delamination is 90% of the length of the lowermost delamination. This difference in the delamination length, upon traversing through the thickness of the CFRP specimen, is attributed to a greater indentation on the surface of the composite occurring when using the round-nosed impactor, as discussed below in detail. To further understand the damage mechanisms, OM and SEM inspections were performed on cross-sections of the post-impacted specimens.

Fig. 9 shows the damage morphology for the round-nosed impactor at an impact energy of 25 J, with matrix cracking, delaminations and fibre pull-out fracture under the impactor being observed. For this round-nosed impactor test, the contact interface between the composite material and the impactor changes from point contact to a full surface contact of the impactor tip as the test proceeds due to indentation of the surface of the composite occurring. The compression and indentation, and subsequent induced shear and tensile stresses, under the round-nosed impactor, leads to matrix cracking followed by delamination and, at relatively high impact energies, also fibre pull-out fracture.

Fig. 10 shows the damage morphology for the flat-ended impactor at an impact energy of 25 J. For the flat-ended impactor, matrix cracking and subsequent delaminations were found to initiate around the circular periphery of the impactor and then to propagate away from the impact point. This left a central area under the impactor with no matrix cracking or delamination occurring, seen as a central dark blue area in the C-scan image, see Figs. 6 and 11. This is due to an effective ring of contact between the edge of the impactor and the CFRP panel. An interesting point is that the damage morphology obtained, from these flat-ended impactor tests, showed that the fibres exhibited a kinking-type fracture, which formed a band of roughly 360 μm in width and was tilted at an approximate angle of 30°. (This angle refers to the angle between the kink-band and a perpendicular, in the plane of the photograph, to the original fibre direction measured in a normal way with a protractor). This zone of kinking fracture occurred around the periphery of the flat-ended impactor.

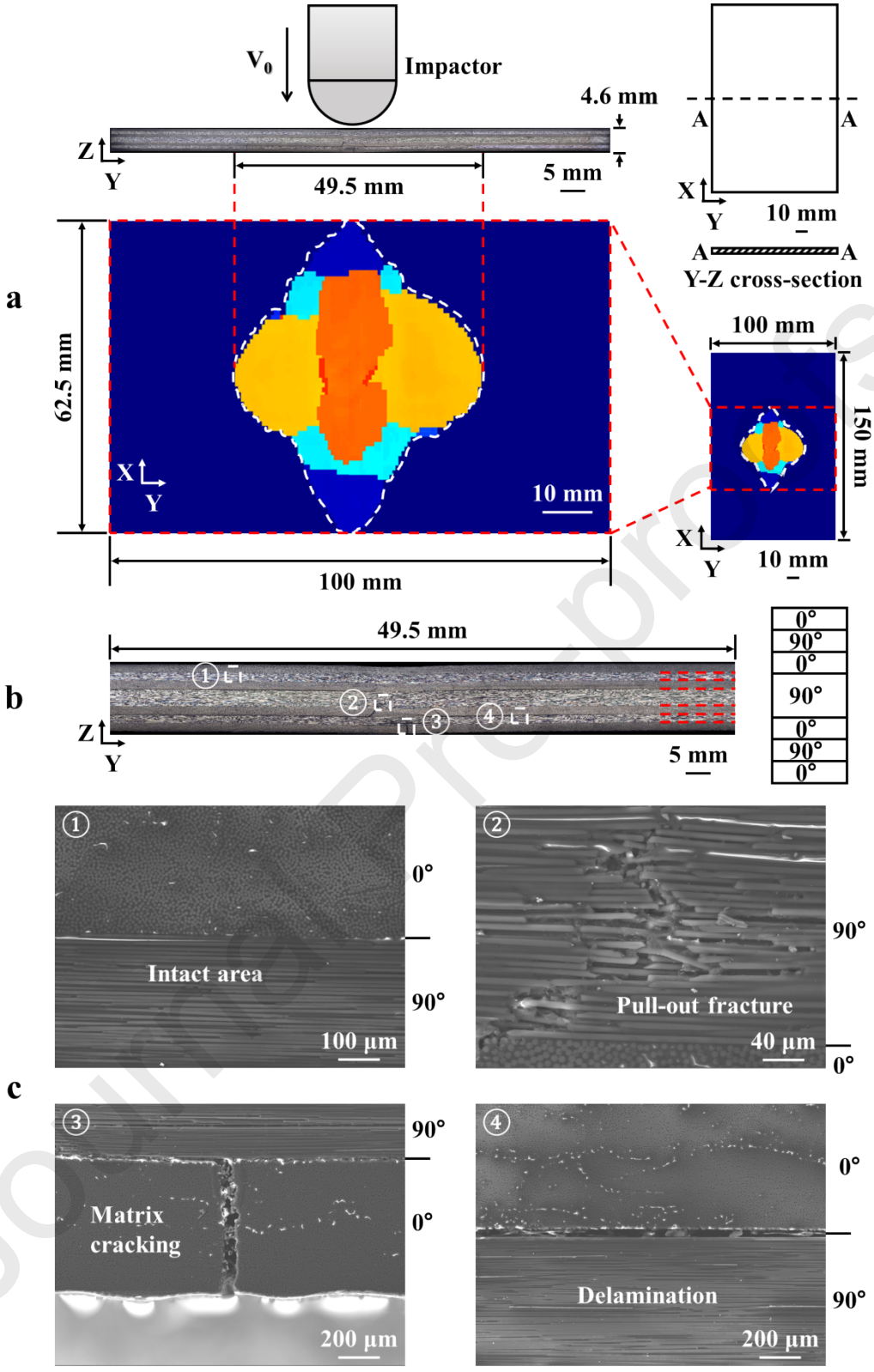

Fig. 9. Cross-section inspection of the panel subjected to an impact energy of 25 J using the round-nosed impactor: (a) the position of inspection; (b) an OM image of the central section; (c) representative damage mechanisms characterised using SEM.

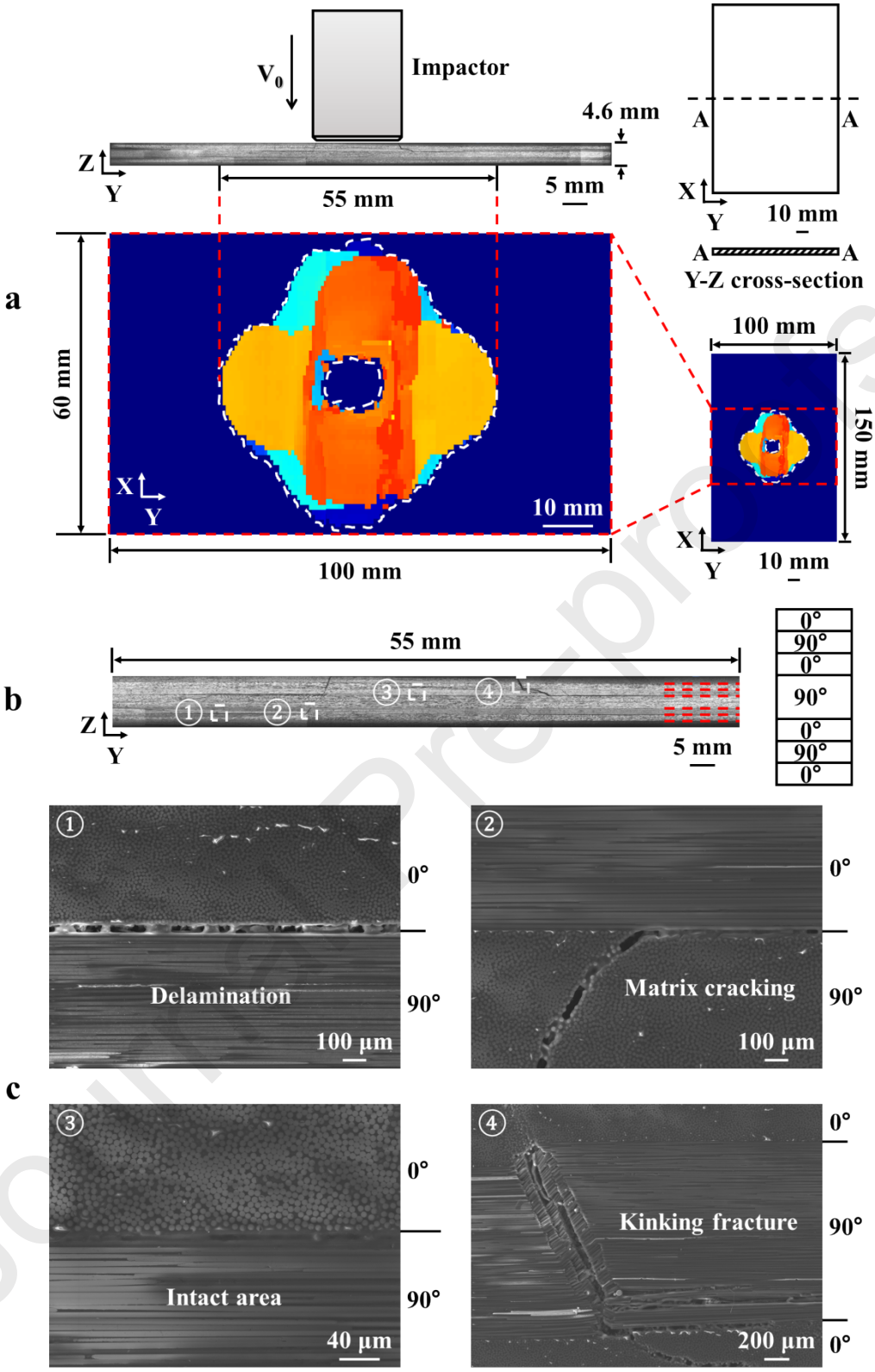

Fig. 10. Cross-section inspection of the specimen subjected to an impact energy of 25 J using the flat-ended impactor: (a) the position of inspection; (b) an OM image of the central section; (c) representative damage mechanisms characterised using SEM.

3.5. Other findings

To obtain more information on the delamination growth with increased impact energy for the flat-ended impactor tests, an additional flat-ended impactor test was performed at an impact energy of 22.5 J. From Fig. 11 it can be seen that, at this impact energy, again there are two separated sub-areas of delamination in the CFRP panel specimen. This arises due to the shorter span length across the width of the panel which means that it has a larger bending stiffness in this direction. The out-of-plane displacement of the CFRP panel specimen tends to generate a larger bending moment and causes a higher interfacial shear stress across the width of the panel, which leads to a relatively early appearance of completely separated delaminations occurring at this impact energy of 22.5 J. At a higher impact energy, these two separate areas of delamination become connected once the shear stresses acting on the length of the panel reach the damage threshold, forming a ring delamination shape with a central non-delamination area, see Figs. 6 and 11. (It should be noted that to examine the reproducibility of these tests, then the flat-ended impacts were conducted using three replicate tests at impact energies of 20, 22.5 and 25 J, with the corresponding C-scan results presented in Fig. 11. The variation in the delamination area at each impact energy is of the order of ±5%, with values of ±3.7% and ±1.3% for the tests at impact energies of 22.5 and 25 J, respectively. These results again demonstrate the good repeatability of the test procedures.)

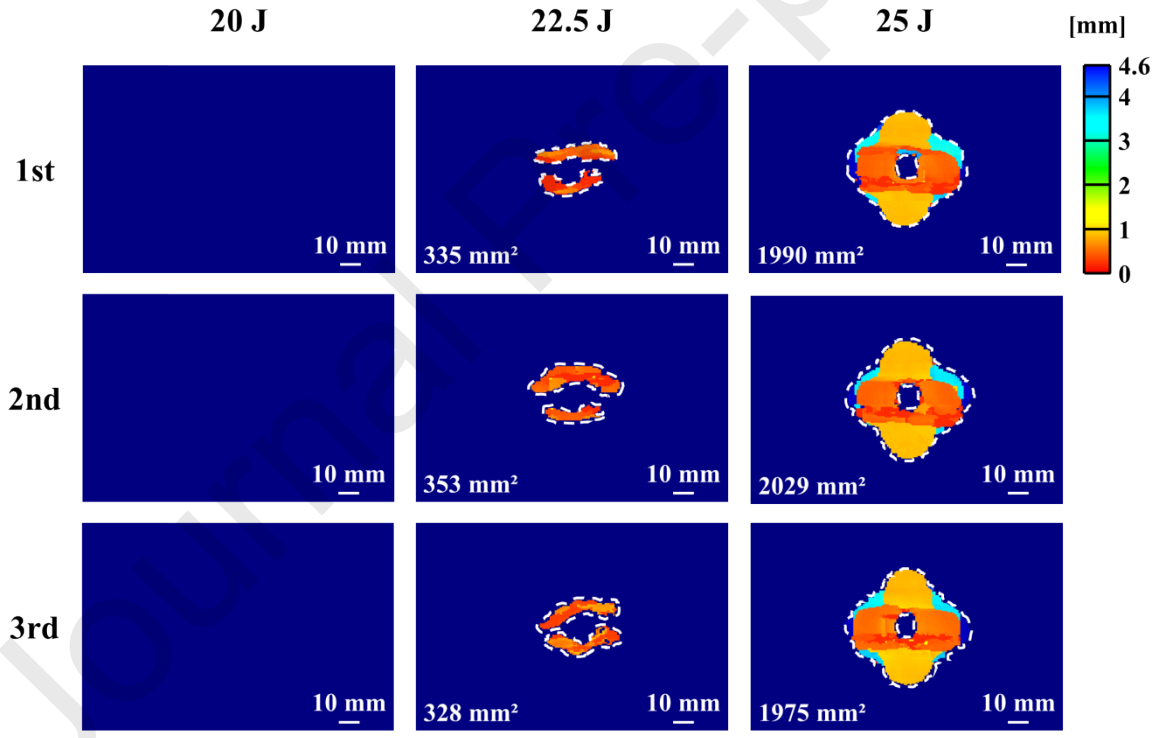

Fig. 11. Comparison of C-scan results for three replicate experiments for the flat-ended impactor at impact energies of 20, 22.5 and 25 J.

It is interesting to note that there is no appreciable major drop in the load versus time trace for the flat-ended impactor at an impact energy of 22.5 J, as shown in Fig. 12, even though some impact delamination damage has initiated, see Fig. 11. Similar results have been reported by Sjöblom et al.[34] and Schoeppner et al.[35]. Therefore, it is important to note that, whilst the

appearance of an appreciable drop in load tends to indicate significant growth of impact-induced damage, such as delaminations, matrix cracking, fibre fracture and indentation, it is clearly possible to have some induced impact damage with no accompanying appreciable load drop. Hence, under some circumstances, slight damage, which may not significantly compromise the structural integrity of the panel, can occur with no appreciable load drop.

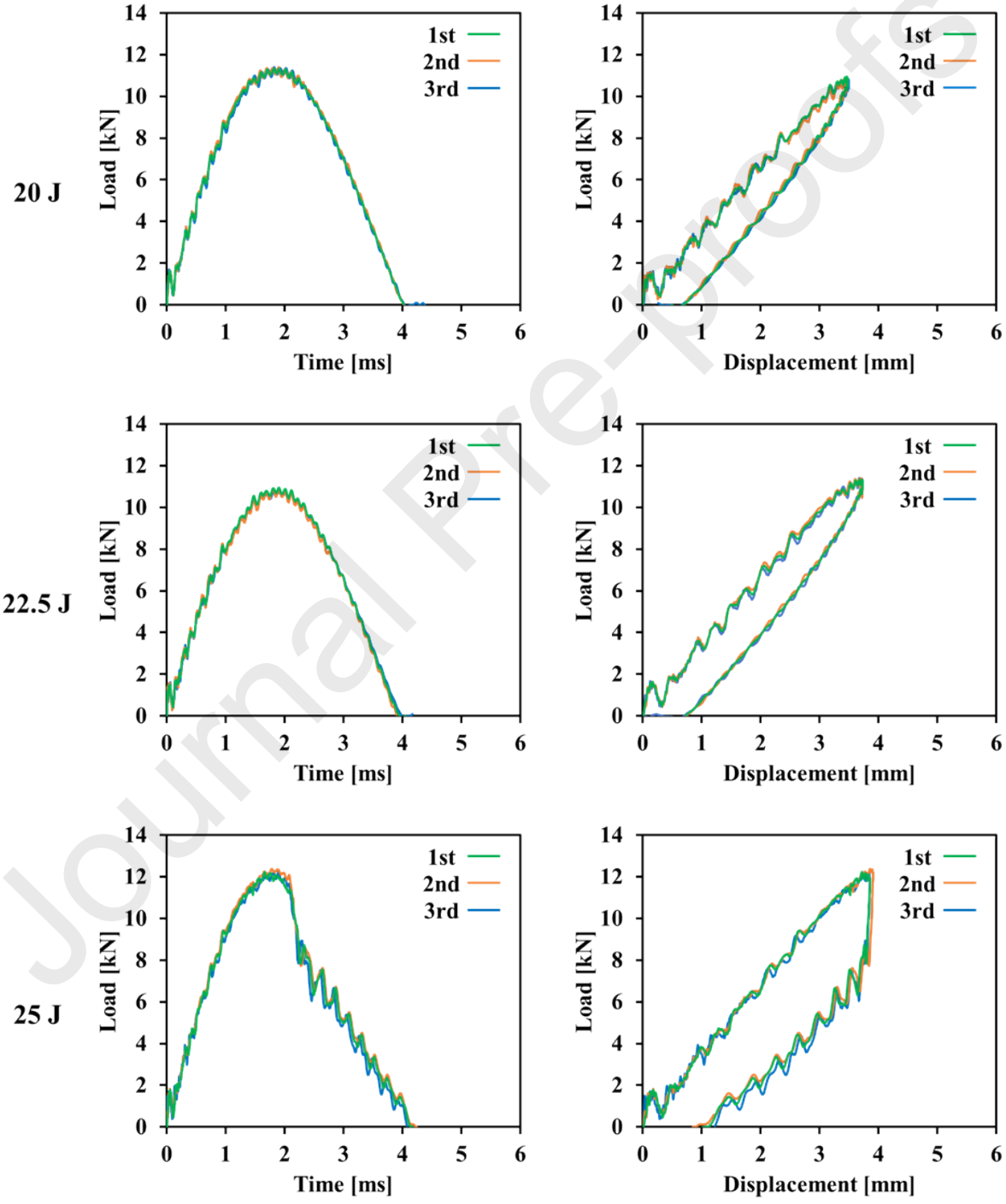

Fig. 12. Comparison between the load-time and load-displacement traces obtained for three replicate experiments for the flat-ended impactor at impact energies of 20, 22.5 and 25 J.

Finally, since the role of any indentation on the impacted face of the CFRP panel specimen influencing the damage mechanisms has been mentioned above, it was useful to study quantitatively the indentation profiles in the impacted faces of the composite panel specimens where permanent (plastic) deformation has been induced in the impacted face of the CFRP. Hence, displacements across the impacted surface were obtained using a non-contact 3D optical profiling tool for surface height measurement, i.e. using white light interferometry (WLI) [36]. The displacement of the surface of the CFRP was measured across the impacted CRFP panel specimen for 20 mm either side of the point of impact, which occurred in the centre of the panel specimen, as shown in Figs. 13 and 14. The depth of the indentation is far much more marked when the round-nosed impactor is used, where the maximum depth of indentation is approximately 200 µm. In comparison, when the flat-ended impactor is used the indentation has a maximum depth of only about 50 µm. However, in the case of the flat-ended impactor, there is a greater build-up of displaced material around the periphery of the impactor. These different indentation profiles associated with the two types of impactor have a significant effect on the resulting delamination and other damage mechanisms, as has been observed and discussed above.

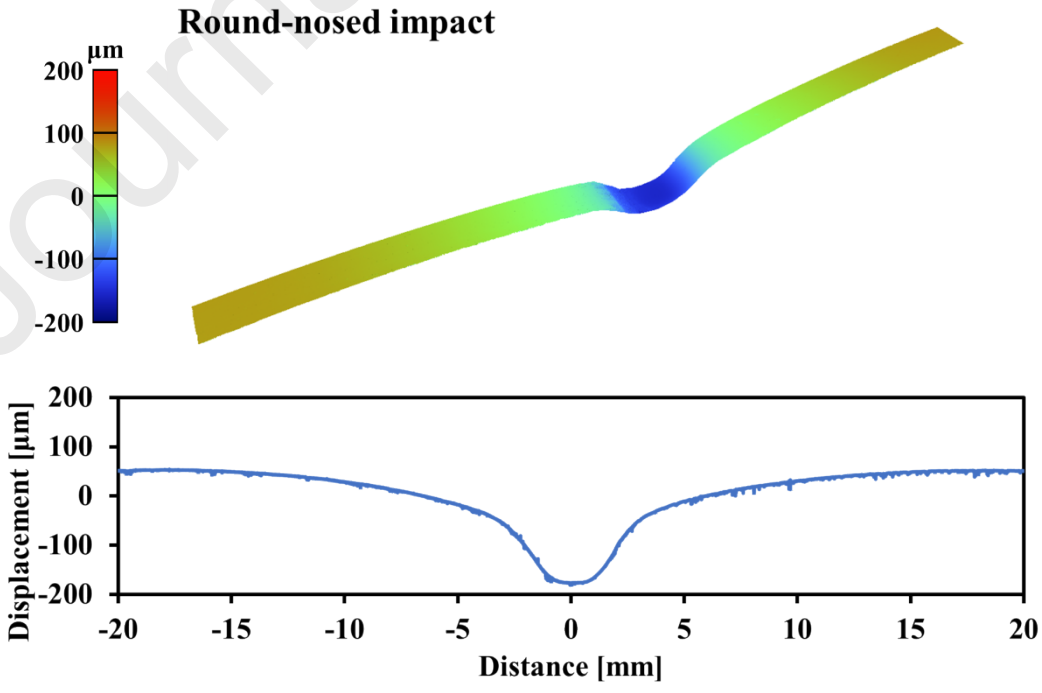

Fig. 13. A white light interferometer (WLI) scan of the indentation profile on the CFRP panel specimen subjected to the round-nosed impactor at an impact energy of 25 J.

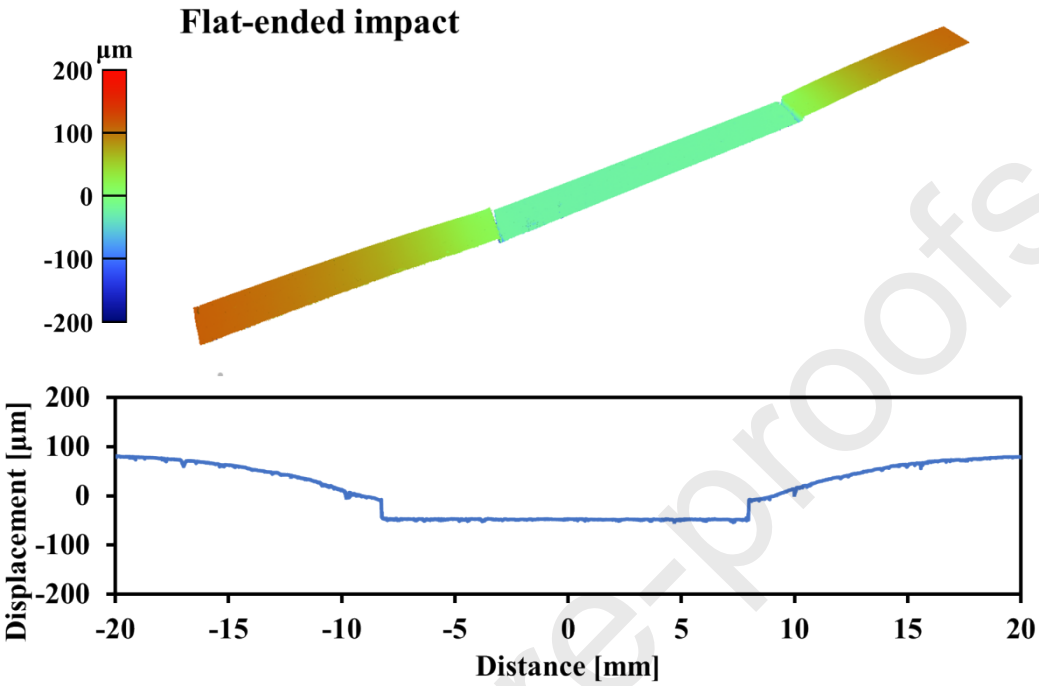

Fig. 14. A white light interferometer (WLI) scan of the indentation profile on the CFRP panel specimen subjected to the flat-ended impactor at an impact energy of 25 J.

4. Conclusions

In the present paper, the impact behaviour of cross-ply CFRP panel specimens struck using either a round-nosed or a flat-ended impactor, at different impact energy levels between 10 and 30 J, has been investigated. The loading responses, delamination areas and damage mechanisms have been studied and compared.

The main findings are:

- The CFRP panel specimens struck using the round-nosed impactor exhibited a relatively longer contact duration, a higher displacement and a lower initial damage load compared with the CFRP specimens struck using the flat-ended impactor.
- The depth of the indentation at the impact point in the impacted face of the CFRP panel specimen is far more marked when the round-nosed impactor is used, where the maximum depth of indentation is approximately 200 μm. In comparison, when the flat-ended impactor is used, the indentation has a maximum depth of only about approximately 50 μm. The degree of indentation induced by the impactor appears to play a significant role in the initiation and development of subsequent damage in the CFRP.
- For the round-nosed impactor, the load for the initiation of damage is approximately 5 kN and this is exceeded at all the impact energies employed. Thus, delamination and other damage in the CFRP specimens is observed at all the impact energies used when the round-nosed impactor is employed. For the flat-ended impactor, which does not promote an indentation of the surface of the CFRP to the same extent as the round-nosed impactor, the load for the initiation of damage is approximately 12 kN and this is only exceeded when the impact energy is above 20 J. Thus, no impact damage is observed in the CFRP specimens when the flat-ended impactor is used at impact energies of 20 J and lower.
- Delaminations in the CFRP panel specimens struck by the round-nosed impactor increase in size with an increasing impact energy from 10 to 30 J. In contrast, for the CFRP specimens struck by the flat-ended impactor, delaminations could only be detected when the impact energy exceeded 20 J.
- The relatively large contact region between the flat-ended impactor and the CFRP specimen resulted in a circular zone of damage but with no delaminations directly beneath the central impact point of the flat-ended impactor.
- The greater level of indentation of the CFRP surface from using the round-nosed impactor resulted in a significant variation of the length and area of a delamination through the thickness of the CFRP specimen.
- At a relatively high impact energy, i.e. greater than 20 J, fibre fracture for the flat-ended impact specimens exhibited a kinking-type fracture just beyond the periphery of the flat-ended impactor. At these impact energies, the panels impacted using the round-nosed impactor tended to show a fibre pull-out failure mechanism.

Acknowledgements

The authors would like to express their appreciation to Dr. Ruth Brooker and Mr. Suresh Viswanathan-Chettiar at Imperial College London, for their valuable support on the experimental testing conducted in this research.

References

1. Roeseler B, Sarh B, Kismarton M. Composite structures—the first 100 years. Boeing 787 Progr Compos Des Tutor 2009;1-4.

2. Soutis C. Fibre reinforced composites in aircraft. Prog Aerospace Sci 2005;41(2):143-51

3. Falzon BG, Pierce RS. Thermosetting composite materials in aerostructures. InRevolutionizing Aircraft Materials and Processes. Springer; 2020, p. 57-86.

4. Caminero M, García-Moreno I, Rodríguez G. Damage resistance of carbon fibre reinforced epoxy laminates subjected to low velocity impact: Effects of laminate thickness and ply-stacking sequence. Polym Test 2017;63:530-41.

5. Patel J, Ayyar A, Peralta P. Kink band evolution in polymer matrix composites under bending: A digital image correlation study. J Reinf Plast Compos 2020;39(21-22):852-66.

6. Cantwell W. The influence of target geometry on the high velocity impact response of CFRP. Compos Struct 1988;10(3):247-65.

7. Cantwell W, Morton J. Geometrical effects in the low velocity impact response of CFRP. Compos Struct 1989;12(1):39-59.

8. Cantwell W, Morton J. Comparison of the low and high velocity impact response of CFRP. Compos 1989;20(6):545-51.

9. Cantwell WJ, Morton J. The impact resistance of composite materials—a review. Compos 1991; 22(5):347-62.

10. Richardson M, Wisheart M. Review of low-velocity impact properties of composite materials. Compos A Appl Sci Manuf 1996;27(12):1123-31.

11. Zhou J, Liao B, Shi Y, Zou Y, Tuo H, Jia L. Low-velocity impact behavior and residual tensile strength of CFRP laminates. Compos B Eng 2019;161:300-13.

12. Mines R, Roach A, Jones N. High velocity perforation behaviour of polymer composite laminates. Int J Impact Eng 1999;22(6):561-88.

13. Icten BM, Kıral BG, Deniz ME. Impactor diameter effect on low velocity impact response of woven glass epoxy composite plates. Compos B Eng 2013;50:325-32.

14. Sevkat E, Liaw B, Delale F. Drop-weight impact response of hybrid composites impacted by impactor of various geometries. Mater Design 2013;52:67-77.

15. Mitrevski T, Marshall IH, Thomson RS, Jones R, Whittingham B. The effect of impactor shape on the impact response of composite laminates. Compos Struct 2005;67(2):139-48.

16. Mitrevski T, Marshall IH, Thomson RS, Jones R. Low-velocity impacts on preloaded GFRP specimens with various impactor shapes. Compos Struct 2006;76(3):209-17.

17. Kurşun A, Şenel M, Enginsoy HM, Bayraktar E. Effect of impactor shapes on the low velocity impact damage of sandwich composite plate: Experimental study and modelling. Compos B Eng 2016;86:143-51.

18. Elaldi F, Baykan B, Akto C. Experimental analysis for the effect of impactor geometry on carbon reinforced composite materials. Polym Polym Compos 2017;25(9):677-82.

19. Kazemianfar B, Esmaeeli M, Nami MR. Response of 3D woven composites under low velocity impact with different impactor geometries. Aerosp Sci Technol 2020;102:105849.

20. Dhakal H, Zhang Z, Bennett N, Reis PNB. Low-velocity impact response of non-woven hemp fibre reinforced unsaturated polyester composites: Influence of impactor geometry and impact velocity. Compos Struct 2012;94(9):2756-63.

21. Mahesh V, Joladarashi S, Kulkarni SM. Influence of laminate thickness and impactor shape on low velocity impact response of jute-epoxy composite: FE study. Mater Today Proc 2020;28:545-50.

22. Liu J, He W, Xie D, Tao B. The effect of impactor shape on the low-velocity impact behavior of hybrid corrugated core sandwich structures. Compos B Eng 2017;111:315-31.

23. Hu Y, Liu W, Shi Y. Low-velocity impact damage research on CFRPs with Kevlar-fiber toughening. Compos Struct 2019;216:127-41.

24. Vitiello L, Russo P, Papa I, Lopresto V, Mocerino D, Filippone G. Flexural properties and low-velocity impact behavior of polyamide 11/basalt fiber fabric laminates. Polym 2021;13(7):1055.

25. Ma S, He Y, Hui L, Xu L. Effects of hygrothermal and thermal aging on the low-velocity impact properties of carbon fiber composites. Adv Compos Mater 2020;29(1):55-72.

26. Liu H, Liu J, Ding Y, Zhou J, Kong X, Blackman BR, Kinloch AJ, Falzon BG, Dear JP. Effects of impactor geometry on the low-velocity impact behaviour of fibre-reinforced composites: an experimental and theoretical investigation. Appl Compos Mater 2020;27(5):533-53.

27. ASTM D 7136. Standard test method for measuring the damage resistance of a fiber-reinforced polymer matrix composite to a drop-weight impact event. Philadelphia, PA: ASTM International; 2012.

28. Liu H, Liu J, Ding Y, Zheng J, Kong X, Zhou J, Harper L, Blackman BR, Kinloch AJ, Dear JP. The behaviour of thermoplastic and thermoset carbon fibre composites subjected to low-velocity and high-velocity impact. J Mater Sci 2020;55(33):15741-68.

29. Dear JP, MacGillivray JH. Strain gauging for accurate determination of K and G in impact tests. J Mater Sci 1991;26(8):2124-32.

30. Crouch BA, Williams JG. Modelling of dynamic crack propagation behaviour in the three-point bend impact specimen. J Mech Phys Solid 1988;36(1):1-13.

31. Williams JG, Adams GC. The analysis of instrumented impact tests using a mass-spring model. Int J Fract 1987;33(3):209-22.

32. Dear JP. High speed photography of impact effects in three-point bend testing of polymers. J Apply Phys 1990;67(9):4304-12.

33. Bienias J, Jakubczak P, Surowska B. Comparison of polymer composites behavior to low-velocity impact and quasi-static indentation. Compos Theory Pract 2013;13(3):155-59.

34. Sjoblom PO, Hartness JT, Cordell TM. On low-velocity impact testing of composite materials. J Compos Mater 1988;22(1):30-52.

35. Schoeppner GA, Abrate S. Delamination threshold loads for low velocity impact on composite laminates. Compos A Appl Sci Manuf 2000;31(9):903-15.

36. Deck L, de Groot P. High-speed noncontact profiler based on scanning white light interferometry. Appl Opt 1994; 33(31): 7334–8.

Declaration of interests

☒ The authors declare that they have no known competing financial interests or personal relationships that could have appeared to influence the work reported in this paper.

☐ The authors declare the following financial interests/personal relationships which may be considered as potential competing interests:

Author statement:

***Yuzhe Ding*:** Methodology, Formal analysis, Writing- Original draft preparation.

***Jun Liu*:** Writing- Reviewing and Editing.

Zoe E.C. Hall: Writing- Reviewing and Editing.

Richard A. Brooks: Writing- Reviewing and Editing.

***Haibao Liu*:** Methodology, Writing-Reviewing and Editing.

***Anthony J. Kinloch*:** Methodology, Writing-Reviewing and Editing.

John P. Dear: Methodology, Writing- Reviewing and Editing, Supervision.